SILICA DOPANT EFFECT ON THE PERFORMANCE OF CALCIUM CARBONATE/CALCIUM OXIDE BASED THERMAL ENERGY STORAGE SYSTEM

Azhar Abbas KHOSA[1], Najam-ul-Hassan SHAH[2], Xinyue HAN[1,]*, Naveed HUSNAIN[3]

[1]School of Energy and Power Engineering, Jiangsu University, Zhenjiang, Jiangsu, 212013, China

[2]Department of Mechanical Engineering, University of Engineering and Technology, Taxila, Pakistan

[3]Department of Mechanical Engineering, Faculty of Engineering and Technology, Bahauddin Zakariya University, Multan 60800, Pakistan

*Corresponding Author; Email:hanxinyue123456@163.com (X. Han)

$CaCO_3$ is being studied for its application in thermal energy storage. However, it has drawbacks of slow reaction rate during calcination and incomplete reversible carbonation which limit its use. In this paper, SiO_2 has been studied as a dopant for $CaCO_3$ to improve its cyclic performance. $CaCO_3$ samples were loaded with different concentrations of SiO_2 and its effect on the thermal energy density of $CaCO_3$ was determined. Afterwards, the effect of the dopant on the heat storage process of the synthesized composite along with kinetics of decarbonation reaction was investigated. Cyclic tests were performed to determine the reusability of the material. It was found that the addition of dopant helped to increase the rate of decarbonation reaction, thereby making the heat storage process more efficient as compared to pure $CaCO_3$. The activation energy values are 255.9, 280.1, 244.9 and 234.8 kJ/mol for 5%, 15%, 30% and 0% doped SiO_2 samples, respectively. Furthermore, thermal energy storage density increases when the amount of dopant decreases in the samples such as the 30% and 5% doped samples have gravimetric energy storage densities of 339.85 and 759.24 J/g, respectively. It was observed that the large quantities (15% and 30%) of dopant had introduced a new phase of Ca_3SiO_5 during $CaCO_3$ decomposition.

Keywords: *Thermochemical heat storage, Catalysis, Kinetics Analysis, Non-isothermal Methods.*

1. Introduction

In recent times, there has been a rapid increase in installation of power plants to harness the renewable energy. This surge is because of the collective decision of the countries attending the 21st Party Meeting, to take measures to limit the global surface temperature rise under 2 °C in the next century [1]. To achieve this crucial objective, a substantial contribution of renewable energy generation must be incorporated into the grid, on an urgent basis. However, the intermittency of renewable energy sources such as solar and wind energy produce a gap between supply and demand of these energies. To achieve a smooth power generation using these energy sources, it is necessary to develop a large-scale energy storage system.

To this end, concentrated solar thermal technology is being developed since it can be combined with a thermal energy storage (TES) system to feed power to the grid day in and day out, replacing the conventional fossil fuel-fired power plants [2-4].In traditional thermal power plants, the thermal energy generated by the combustion of fossil fuels is used to produce supersaturated steam, which passes through the rotary turbine to yield mechanical power. Whereas in a concentrated solar power plant (CSP), the solar radiation is concentrated by a field of reflecting surfaces called heliostats on to a receiver at the top of a tower. The receiver consists of a heat exchanger that transfers thermal energy to a working medium (such as a molten salt). This working medium in turn generates steam to run the turbine. The traditional furnace-boiler system in the thermal power plants is thus replaced by a concentrator-receiver-generator system in the CSP plant to harness solar energy. Currently, numerous CSP plants incorporated with the TES are operating worldwide to generate electricity for commercial use.

On sunny days, the concentrated solar beam directly heats up the molten salt mixture, which can be utilized for electricity generation or stored for later use in a TES system. Commonly known TES systems are latent and sensible heat storage systems, which are widely studied for their various applications [5-10]. In sensible heat storage system, the high-temperature salt mixture is stored in a well-insulated tank. When needed, the stored energy is provided to a steam generator for steam generation and a separate tank is used to store the cooled salts. Binary, ternary and two ternary molten salts based systems, which are used commonly in TES are KNO_3-$NaNO_3$, $NaNO_2$-$NaNO_3$-KNO_3 and $Ca(NO)_3$-$NaNO_3$-KNO_3, $LiNO_3$-KNO_3-$NaNO_3$, respectively. Molten salts used in TES systems are reviewed concisely and comprehensively in these studies [11-14]. In a typical sensible heat storage, an energy storage density of about 0.8 GJ/m^3 is achieved [15].

Owing to some complications associated with the energy storage systems using molten salts incorporated with CSPs, the attractiveness of these systems is impeded. One of the difficulties is that the salt decomposes above 600 °C. This prevents from achieving higher temperatures in such systems, which in turn, limits their Carnot efficiency as compared to the conventional power plants. Another problem is that the solidification temperature (120-220 °C) of molten salts is well above the ambient temperature. This sets a limit for the lowest operating temperature of the molten salt and requires external heating of the piping at night resulting in a drop in efficiency due to heat losses for power plants installed in high altitude deserts. Moreover, the requirement of non-corrosive materials, to avoid corrosion problems due to salts, makes the installation of power plant costly.

In a latent heat storage system, the working fluid (molten salt mixture) exchanges heat with another material typically an encapsulated phase change material (PCM) with a high melting temperature [16-22]. Energy is stored in the molecular bonds by melting the PCM. When energy is needed, the working fluid at low temperature extracts energy from the PCM resulting in its solidification. These systems offer several advantages over the sensible heat based TES, such as high storage density and less temperature fluctuations. However, they also have some disadvantages such a complicated TES design, higher cost, corrosivity of inorganic PCMs towards most metals, decomposition and subcooling which can affect their performance. Both the sensible and latent heat-based TES systems have a lower energy storage density compared to the thermochemical energy storage system (TCES). Furthermore, the energy losses of both the sensible and latent heat-based storage systems increase with the storage duration, and they are not suitable for seasonal storage despite heavy insulation. Therefore, it is necessary to explore a new energy storage method such as

TCES that is cheaper, more reliable, easily scalable for large plants and can handle seasonal storages efficiently.

TCES system that stores heat in the chemical form is in its early development phase and can substitute molten salt based and the PCM based TES systems [23, 24]. TCES stores heat as a result of an endothermic forward reaction, which occurs at high temperatures and can be carried out using concentrated solar heat. Energy is released when the individually stored products of the reaction are allowed to react exothermically in reverse direction. TCES has a higher energy storage density compared to other storage systems. The products of forward endothermic reaction can be separated from each other and stored everlastingly allowing seasonal storage. TCES can achieve much higher storage and retrieval efficiencies, when a proper reaction system according to the application temperature is selected [25].

A key task is to select a reaction pair closely matching the requisites of a solar tower power plant. The reaction system must have a low operational cost and affordable capital and material costs. Similarly, the operational temperature range of the system and the turning temperature of the reaction pair must match each other for proper selection [26]. Keeping in view these requirements, the process of calcium-looping (CaL) is selected for further study [27]. The forward and reverse reaction of CaO with CO_2 in the 'simple' CaL process are (Eq. (1)).

$$\boldsymbol{CaCO_3 + 177.8\ kJ/mol \leftrightharpoons CaO + CO_2} \quad (1)$$

In another CaL process, $Ca(OH)_2$ is used. Calcium hydro-oxide and calcium carbonate are preferred because they are cheap, abundantly available and safe. They form no byproducts during the reaction, and they have a higher energy storage density compared to other materials; as for $Ca(OH)_2$ and $CaCO_3$ it is 0.39 and 0.49 kWh/kg, respectively [25]. $CaCO_3$/CaO pair have a high reaction temperature (890 °C), which makes it suitable for high temperature applications like concentrated solar power plants. The $CaCO_3$ shows many advantages over $Ca(OH)_2$, it has a higher reaction enthalpy (177.8 kJ/mol) compared to 109 kJ/mol for $Ca(OH)_2$. It produces gaseous CO_2 and powdered CaO, which are normally stable at room temperature. Moreover, it can store thermal energy for a long time [28].

In $CaCO_3$ TCES system, heat storage and release processes are crucial because over multiple cycles its reactivity declines. Variables that influence the performance of this system are residence time [29], particle size [30], temperature [31] and atmosphere [32]. It was found that the reactivity of solid particles can be enhanced by adding dopants in the pure material. In this regard, Shui *et al.* [33] studied the effect of SiO_2 dopant on the calcination of $CaCO_3$, which reveals that pure $CaCO_3$ sample followed the contracting sphere model and the doped sample calcined according to the one-dimensional diffusion model. Further, the dopant helped trigger the calcination at a lower activation energy of 155 kJ/mol. This is because SiO_2 can absorb high amounts of heat and helps $CaCO_3$ to retain pores by resisting grain accumulation. On the contrary, Kumar *et al.* [34] doped SiO_2 in calcium carbonate with 0.25%, 1% and 2% amounts and determined that less amount of dopant (0.25% and 1%) leads towards lower activation energy and vice versa. Similarly, Chen *et al.* [35] reported that when the amount of SiO_2 dopant is increased above 5%, the activation energy also increases, which makes it hard to achieve a reasonable reaction rate. Valverde *et al.* [36] reported that CaO grain accumulation can be avoided by doping nano-silica and thermal pre-treatment of calcium carbonate. This process can help calcine the material at low CO_2 pressures and moderate reaction temperatures.

The effect of some other dopants on this system was also reported, for example, CeO_2 [37] and AlOOH [38] lowered the activation energy of the reaction to 40 and 90 kJ/mol, respectively.

In addition to all above-mentioned parameters, a multi-cycle cyclic stability study for the material is mandatory, which helps decide whether the material is a suitable candidate for commercial use or not. In this regard, Barker [39] reported a gradual degradation of $CaCO_3$ after 40 cycles of heat storage and release processes at 866 °C. Further, the author reported that calcination reaction was always complete, but the carbonation was incomplete because of inactivity of CaO. Erans *et al.* [40] suggested that performing the hydration of CaO after some cycles can help improve its reactivity by 35-40%. This technique is not feasible because hydration reaction is performed at lower temperatures while the calcination is carried out at higher temperatures. On the contrary, it was reported that dopants such as Li_2SO_4 [41], $Ca_3Al_2O_6$ [42] and TiO_2 [43] can increase the reactivity of CaO in multi-cycle process by resisting CaO grain accumulation and help retain its porosity for CO_2 diffusion. In another study by Benitez-Guerrero, M., *et al.* [44], it was found that dolomite, which contains MgO as impurity produced better reactive CaO as compared to CaO formed by calcination of marble and limestone. Chen *et al.* [45] doped CaO with MnO_2 and MgO, which led to storage conversion of 0.76 and 0.79, respectively, for 50 cycles. Consequently, we can conclude that addition of dopants is useful for efficient performance of $CaCO_3$ TCES system in multi-cycle applications. A list of dopants with their thermophysical properties is provided in Tab. 1.

Table 1. Thermophysical properties of some dopants that are used with $CaCO_3$

Dopant	Thermal Conductivity (W/m K)	Heat Capacity (J/mol K)
Li_2SO_4	-	1.07 (J/g K) [46]
MgO	45-60 [47]	37.2 [48]
MnO_2	-	54.1 [49]
SiO_2	10.2 [50]	-

From the above-mentioned studies, it is clear that the $CaCO_3$/CaO system has particles sintering problem after being treated at high temperatures, which leads to incomplete carbonation reaction. Literature of using SiO_2 as a dopant [33-35] has mixed results regarding its effect on $CaCO_3$ at higher concentrations. In the study by Chen *et al.* [35], the effect of SiO_2 dopant on thermodynamic properties of the $CaCO_3$ has been discussed but not on the TCES system performance. Additionally, studies using SiO_2 as dopant [33-36, 51] have not determined the thermal energy storage density of the samples. In this paper, we investigate the use of SiO_2 as a dopant and study its effect in large amounts (5%, 15% and 30%) on the TCES system. Furthermore, we also study the volumetric and gravimetric thermal energy densities of the $CaCO_3$/CaO system doped with SiO_2, effect of dopant on the reaction kinetics, and observe the formation of a new phase [52] due to reaction between SiO_2 and $CaCO_3$ at 800 °C.

In this regard, we have performed non-isothermal kinetics study on the pure as well as doped $CaCO_3$ and analyzed the effect of large amount of dopant on the heat storage properties of the material. We used X Ray Diffraction (XRD) technique to determine if a new phase appears during reaction due to large amount of dopant used. We examined the durability of the material by performing repeated cycles of carbonation and decarbonation reactions. Additionally, we determined the volumetric and gravimetric thermal energy densities of all the prepared samples.

2. Materials and methodology

$CaCO_3$ and SiO_2 (99.5% purity with particle size of 15 nm) were purchased from Sinopharm Chemical Reagent Company Limited and Aladdin Industrial Corporation, respectively. The proximate analysis of $CaCO_3$ is provided in our published study [53]. For the preparation of $SiO_2/CaCO_3$ thermal composite, three different concentrations of SiO_2 (5%, 15% and 30%) were used and the mixing was performed as described in our previous work [53]. Both pure and SiO_2-doped samples of calcium carbonate were analyzed through simultaneous temperature analyzer (STA8000 of PerkinElmer). The prepared powder samples were heated non-isothermally up to 900 °C by using three different heating rates of 5, 10 and 15 °C/min, and 650 °C was selected as the initial temperature because the decarbonation starts after this temperature. After approaching the maximum temperature (900 °C), the samples were heated constantly for 10 min to allow complete decomposition of material. Argon gas with high purity (99.999%) was introduced at a flow rate was 50 ml/min.

All prepared samples were tested in the STA to obtain cyclic stability analysis. The sample size was maintained between 9.5±0.5 mg. During calcination process, samples were heated at a rate of 50 °C/min in an inert atmosphere of Argon gas (99.999%) at 800 °C for 10 minutes. Carbonation process was carried out for 10 min in highly pure carbon dioxide environment where samples were cooled down to 600 °C at a rate of 50 °C/min. The flow rates of Ar and CO_2 were 50 ml/min and 100 ml/min, respectively. After the completion of first cycle of decomposition and synthesis of $CaCO_3$, the process was repeated by heating the samples from 600 °C to 800 °C for decarbonation. In this way, 15 cycles were performed.

The materials were analyzed at room temperature for the identification of phases and crystalline structure using XRD from Da Vinci modelled D8 ADVANCE.

2.1. Error Analysis

Error analysis was performed to assess the accuracy of calculations. The equation to calculate system error is as follows:

$$u_s = \sqrt{\left(\frac{\partial h}{\partial T}.u(T)\right)^2 + \left(\frac{\partial h}{\partial X}.u(X)\right)^2} \quad (2)$$

where *u(T), u(X)* are the percentage inaccuracies in the temperature and weight respectively. The $\frac{\partial h}{\partial T}$ and $\frac{\partial h}{\partial X}$ are the differential values of the temperature rise and the reaction progress, respectively.

The electronic balance of the STA has a weight inaccuracy of 0.0001 mg, so *u(X)* will be ±0.0013%; while the inaccuracy in temperature is about 0.01 °C and so *u(T)* will be ±0.0025%.

Now, the error analysis for the activation energy E can be calculated with the following equation:

$$u_E = \sqrt{(u_s)^2 + (u_{fit1})^2} \quad (3)$$

where, u_{fit1} is defined as the fitting error for *E*.

3. Results and discussion

3.1. Structural analysis

For better understanding the phases and crystal lattice of the pure and composite samples of $CaCO_3$, they were analyzed by XRD. The samples were analyzed before heating at decomposition temperature and the diffraction patterns of all the SiO_2-doped samples were in accordance with the pure $CaCO_3$ as presented in the Fig. 1(a). The same was observed when XRD results were imported to the Jade 6.5 software and compared with the peaks available in the software. The structural phases and the planes obtained from XRD were in accordance with the JCPDS card number 05-0586. Hence, it was established that all the peaks are in line with the pure phase and that no secondary phase appeared in the samples during the mixing process. Chen *et al.* [35] used the ball milling method for mixing and they also did not find any other secondary phase after mixing. The reflection planes of $CaCO_3$ doped with SiO_2 crystal phase are clearly indexed in Fig. 1(a). The SiO_2 acted as a heat receptor and helped to enhance the heat absorbing properties of the parent material by causing cracks in the crystal lattice of the $CaCO_3$.

XRD patterns of the calcined samples are presented in Fig. 1(b). The decomposition of all the samples was observed in the form of CaO (JCPDS card number 48-1467). Additionally, another minor secondary phase Ca_3SiO_5 (JCPDS card number 31-0301) was observed in the samples doped with 15% and 30 % of SiO_2, this matches well with Wang *et al.* [54]. Samples with the high amount of dopant depicted another phase (Ca_3SiO_5); the new phase is stable, and it does not affect the performance of the material. Moreover, it also helps in the reversibility of the reaction at much lower temperatures [52]. The same effect was also observed during the cycling test performed on the samples. The samples with Ca_3SiO_5 depicted a remarkable performance and their reversibility to carbonate was easier and faster.

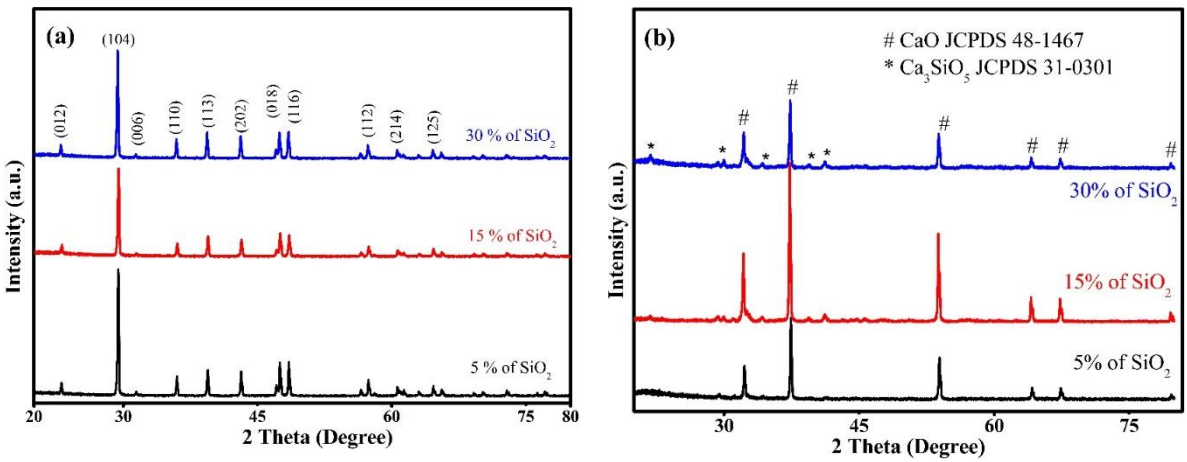

Figure 1. XRD structural analysis of $CaCO_3$ doped with different concentration of SiO_2 (a) before decomposition (b) after decomposition

3.2. Thermal energy density

The thermal energy density is measured in two forms : one based on a unit volume is named as volumetric thermal energy density e_v [J/mL] (Eq. (4)[55]) whereas the other based on a unit-mass of the substance is known as gravimetric thermal energy density e_g [J/g] (Eq. (5)[55]).

$$e_v = \frac{-\Delta H \rho (100 - \varepsilon)}{M_{CaCO3} + M_{SiO2}} \div 100 \quad (4)$$

$$e_g = \frac{-\Delta H}{M_{CaCO3} + M_{SiO2}} \quad (5)$$

Where $-\Delta H$ is the reaction enthalpy [J/mol] of the CaL process and it was determined using thermogravimetric data. M is the molar mass [g/mol] of the composites SiO_2 (60.08) and $CaCO_3$ (100.09). Porosity ε [%] was measured using gravimetric method for the samples. Density ρ [g/mL] of the samples was calculated after weighing them with known volumes. Tab. 2 provides the information about the volumetric and gravimetric thermal energy densities of each sample under consideration.

From Tab. 2, it can be observed that both the volumetric and gravimetric thermal energy storage densities decrease sharply with the increase in the amount of dopant. This can be explained by the lower density of SiO_2 used as a dopant in these samples. Furthermore, the increasing content of SiO_2 decrease the reactant ($CaCO_3$) for thermochemical energy storage.

Table 2. Volumetric and gravimetric thermal energy densities of each sample under analysis

Sample	$-\Delta H$ [J/mol]	ρ [g/mL]	ε [%]	e_v [J/mL]	e_g [J/g]
Pure $CaCO_3$	94609.07	0.59	44.44	311.09	945.24
$CaCO_3$+5% SiO_2	121663.5	0.42	51.22	155.35	759.59
$CaCO_3$+15% SiO_2	79431.51	0.30	44.64	83.24	495.92
$CaCO_3$+30% SiO_2	54433.77	0.28	41.67	54.75	339.85

3.3. Non-isothermal kinetics of the decarbonation reaction

The general equation for the non-isothermal solid and gas reactions, recommended by ICTAC committee is presented in Eq. (6) [56]. This equation is used to calculate the reaction rate using Arrhenius parameters at any given temperature for any heating rate.

$$\frac{dX}{dT} = \left(\frac{A}{\beta}\right) exp\left(-\frac{E}{RT}\right) f(X) \quad (6)$$

In this equation, X is the conversion of reactants into products, R is the ideal gas constant (J/mol K), β is the rate at which material is being heated (°C/min), A is the pre-exponential factor or frequency factor (s^{-1}), E is the activation energy (kJ/mol), T is the temperature (°C or K), and $f(X)$ is a function of conversion of the material. Conversion X is calculated with the help of Eq. (7) [56] as expressed below:

$$X = \left(1 - \frac{w_t}{w_0}\right) \times \frac{M_{CaCO_3}}{M_{CO_2}} \quad (7)$$

Where, w_t represents the weight of material at any time during the reaction, w_0 is the initial weight of the material under analysis, M_{CaCO3} and M_{CO2} are the molecular masses of the calcium carbonate ($CaCO_3$) and carbon dioxide (CO_2), respectively.

3.4. Recognition of the suitable model

In order to determine non-isothermal behavior of pure $CaCO_3$ and as-prepared thermal composites, two models were used namely Coats-Redfern integral method (CRF method) [57] and Achar-Brindly-Sharp differential method (ABS method) [58].

CRF method
$$\boldsymbol{ln\left[\frac{g(X)}{T^2}\right] = ln\left(\frac{AR}{\beta E}\right) - \frac{E}{RT}} \quad (8)$$

ABS method
$$\boldsymbol{ln\left[\frac{d(X)}{f(X)dT}\right] = ln\left(\frac{A}{\beta}\right) - \frac{E}{RT}} \quad (9)$$

Where, *g(X)* is the integral form of the function of the conversion of the material and *f(X)* is the function of the conversion of the material in differential form. All other parameters are as described earlier. Next, we explain the procedure of calculating the pre-exponential factor *A* and activation energy *E* using the above equations.

We used the reaction kinetics models suggested by Vyazovkin *et al.* [56] as specified in the Tab. 3 to determine the best suited model for the decomposition reaction of $CaCO_3$. The term on the left-hand side of the Eq. (8) and (9), was plotted on a graph as an ordinate against 1/T from second term of the right-hand side of the same equations as abscissa. The value of pre-exponential factor *A* was computed from the intercept of the fitting line whereas the activation energy E was calculated from the slope of the fitting curve. The slope and the intercept of the fitting line were calculated using the regression analysis. In the kinetics calculations of the models, the thermogravimetric data obtained from the non-isothermal experiments performed at different temperature rising rates of 5, 10 and 15 °C/min, was used.

Table 3. Some common gas-solid reaction kinetics models. f(X) is the differential form of the conversion function and g(X) is the integral form of the conversion function

Model	Code Name	*f(X)*	*g(X)*
Avarami-Erofeev	A2	$2[-\ln(1-X)]^{1/2}(1-X)$	$[-\ln(1-X)]^{1/2}$
Avarami-Erofeev	A3	$3[-\ln(1-X)]^{2/3}(1-X)$	$[-\ln(1-X)]^{1/3}$
Contracting cylinder	R2	$2(1-X)^{1/2}$	$1-(1-X)^{1/2}$
Contracting sphere	R3	$3(1-X)^{2/3}$	$1-(1-X)^{1/3}$
Mample (1st order)	F1	$(1-X)$	$-\ln(1-X)$
One-dimensional diffusion	D1	$\frac{1}{2}X^{-1}$	X^2
Two-dimensional diffusion	D2	$[-\ln(1-X)]^{-1}$	$(1-X)\ln(1-X)+X$
Three-dimensional diffusion	D3	$\frac{3}{2}\left[1-(1-X)^{1/3}\right]^{-1}(1-X)^{2/3}$	$[1-(1-X)^{1/3}]^2$

3.5. Kinetics of Pure $CaCO_3$

We calculated the kinetics parameters using the models mentioned in Tab. 3. For determining the best model, curve fitting and regression analysis was performed and a model with the highest value of R^2 was selected, while considering closely related R^2 values for CRF and ABS. Tab. 4 lists the best three models for each type of sample whereas Tab. 5 lists the best model selected for each sample type and provides details of reaction kinetics parameters for that model for different heating rate and method used. In our case for pure calcium carbonate, one-dimensional diffusion "D1" was the best suited model based on value of R^2 from the three shortlisted models shown in Tab. 4. The kinetics parameters associated with the D1 model are specified in Tab. 5 corresponding to three

different heating rates and the two methods. The final values of each kinetic parameter were calculated by averaging the different values for the same parameter. For the pure $CaCO_3$, the average value of *E* (activation energy) is calculated 234.8 kJ/mol and corresponding value for pre-exponential factor is 2.15×10^{14} s^{-1}. The final kinetics control equation that provides the reaction rate at any temperature is given as follows:

$$\frac{dX}{dt} = (\mathbf{2.15 \times 10^{14}}) \times exp\left(-\frac{\mathbf{234798.7}}{RT}\right) \times \frac{1}{2}X^{-1} \quad (10)$$

Table 4. Comparison of shortlisted models for decarbonation reaction of pure and doped calcium carbonate samples

Sample	Model	Mean of R^2 (CRF Method)	Mean of R^2 (ABS Method)
$CaCO_3$	D2	0.992	0.978
	R3	0.984	0.991
	D1	0.992	0.985
$CaCO_3$+5%SiO_2	D2	0.992	0.985
	R2	0.990	0.982
	R3	0.991	0.986
$CaCO_3$+15%SiO_2	D2	0.993	0.982
	F1	0.993	0.987
	D3	0.995	0.989
$CaCO_3$+30%SiO_2	F1	0.994	0.975
	A3	0.989	0.975
	D3	0.996	0.990

Table 5. Kinetics parameters for the decarbonation reaction of pure and doped calcium carbonate samples

Sample	β	CRF Method			ABS Method			Model
		E (kJ/mol)	lnA	R^2	E (kJ/mol)	lnA	R^2	
$CaCO_3$	5	292.53	33.17	0.996	225.68	24.98	0.989	D1
	10	311.18	34.58	0.992	228.60	24.65	0.989	
	15	173.05	18.22	0.989	177.75	19.20	0.976	
	mean	258.92	28.66	0.992	210.68	22.94	0.985	
$CaCO_3$+5%SiO_2	5	370.77	41.95	0.990	275.13	30.19	0.991	D2
	10	213.31	22.70	0.993	225.48	24.50	0.982	
	15	258.02	28.22	0.994	192.50	20.51	0.983	
	mean	280.70	30.96	0.992	231.03	25.07	0.985	
$CaCO_3$+15%SiO_2	5	363.84	40.51	0.995	283.83	30.68	0.991	D3
	10	294.83	30.99	0.996	261.46	27.15	0.989	
	15	254.15	26.36	0.994	222.39	22.82	0.985	
	mean	304.27	32.62	0.995	255.89	26.88	0.989	
$CaCO_3$+30%SiO_2	5	285.91	31.49	0.997	252.54	27.49	0.995	D3
	10	263.11	27.53	0.997	220.39	22.51	0.991	
	15	236.75	23.99	0.994	210.68	21.10	0.986	
	mean	261.92	27.67	0.996	227.87	23.70	0.990	

3.6. Kinetics of SiO_2 doped $CaCO_3$

For calculation of kinetics parameters for SiO_2-doped $CaCO_3$, the same procedure was used as for the pure $CaCO_3$. For $CaCO_3$ doped with 5% SiO_2, the D2 model was found the best because of its statistically significant correlation coefficient value and the closely related CRF and ABS outcomes. The comparison of the three short-listed models using R^2 values is given in Tab. 4 and the kinetics parameters associated with the selected D2 model are specified in Tab. 5. The average values of Activation energy (*E*) and the pre-exponential factor (A) are computed as 255.9 kJ/mol and 2.75×10^{17} s^{-1}, respectively. The final kinetics control equation that provides the reaction rate at any temperature is given below:

$$\frac{dX}{dt} = (2.75 \times 10^{17}) \times exp\left(-\frac{255866.9}{RT}\right) \times [-\ln(1-X)]^{-1} \quad (11)$$

For $CaCO_3$ doped with 15% and 30% SiO_2 (higher quantity), the D3 model was found the best because of its statistically significant correlation coefficient value and closely related CRF and ABS outcomes. Following the same procedure as before, Activation energy (*E*) is computed as 280.1 kJ/mol for the 15% SiO_2 doped sample and 244.9 kJ/mol for the 30% SiO_2 doped sample while the value of associated factor *A* is 6.52×10^{16} s^{-1} for the 15% SiO_2 doped sample and 8.23×10^{12} s^{-1} for the 30% SiO_2 doped sample. The final kinetics control equations that provide the reaction rate at any temperature for the 15% and 30% doped silica samples, respectively, are given below:

$$\frac{dX}{dt} = (6.52 \times 10^{16}) \times exp\left(-\frac{280085.9}{RT}\right) \times \frac{3}{2}(1-X)^{2/3}\left[1-(1-X)^{1/3}\right]^{-1} \quad (12)$$

$$\frac{dX}{dt} = (8.23 \times 10^{12}) \times exp\left(-\frac{244897.1}{RT}\right) \times \frac{3}{2}(1-X)^{2/3}\left[1-(1-X)^{1/3}\right]^{-1} \quad (13)$$

Models for the reaction kinetics for the decomposition of the pure and the SiO_2-doped $CaCO_3$ are very different from each other. Pure $CaCO_3$ follows the D1 model, whereas the sample with 5% SiO_2 follows the D2, and the samples with 15% and 30% SiO_2 follow the D3 model for the decomposition reaction. According to these models, the reaction kinetic parameters are also different. Tab. 6 lists the activation energies for the $CaCO_3$ doped with different concentration of SiO_2 for the current study and compares with other researchers. Fig. 2 presents the change in activation energy for the current study with the increase in doping ratio. The activation energy initially increases with the increase in SiO_2 doping from 234.8 kJ/mol for pure $CaCO_3$ to 255.9 and 280.1 kJ/mol for the 5% and 15% SiO_2-doped samples. However, it decreases with further doping of SiO_2 from 15% to 30% by a value of 35.2 kJ/mol.

Table 6. List of activation energies achieved by other researchers after doping inert materials

Inert material used as dopant	Activation energy (kJ/mol)	
	Pure	Doped
AlOOH [38]	210	301.4
SiO_2 [35]	253.7	212.9
CeO_2 [37]	107	40
SiO_2 [Current study, 5%]	234.8	255.9
SiO_2 [Current study, 15%]	234.8	280.1
SiO_2 [Current study, 30%]	234.8	244.9

3.7. Cyclic Stability and Material Performance

For assessing the performance and durability of a thermochemical material over repeated cycles, cyclic tests are conducted. In our tests, the decomposition of the material was performed at 800 °C for 10 min and the carbonation was performed at 600 °C for the same time duration except by changing the gas from Ar to CO_2. The same process was repeated to achieve 15 cycles of decarbonation and carbonation of $CaCO_3$ as shown in the Fig. 3 (curves A, B, C and D are present work). In Fig. 3, cyclic conversion of pure as well as doped $CaCO_3$ is presented together with the results of other researchers for comparison.

It is observed that conversion to carbonate is decreases rapidly in pure $CaCO_3$ (curve A), and the samples doped with 5% SiO_2 up to the seventh cycle. After that, the reactivity of CaO stabilizes slowly and moves towards a persistent value after the completion of 15th cycle. For the 15% doped sample (curve C), the value of the cyclic conversion keeps on declining up to 10 cycles and then stabilize at a value of 0.48. The 5% SiO_2-doped $CaCO_3$ sample (curve B) shows a better cyclic stability and a higher conversion of 0.62 after 15 cycles compared to other samples. This value of SiO_2-doping (5%) is therefore, recommended, for thermochemical heat storage systems using $CaCO_3$.

The cyclic conversion of $CaCO_3$ decreases because CaO loses pores over multiple cycles, which restricts the diffusion of the gas through these pores [39]. This leads to less material available for reaction with CO_2 for heat release process in the subsequent cycle. Furthermore, the carbonate layer, formed as a result of surface reaction between solid particles and gas, slows down the reaction by resisting the further diffusion of CO_2 into the material [35]. Hence, continuous sintering of particles over multiple cycles leads to low cyclic stability of $CaCO_3$. The dopant controls the particle boundary movement by inducing a Zener pinning force, which results in low sintering of CaO particles [35]. Therefore, addition of SiO_2 up to 5% increases the robustness of the material.

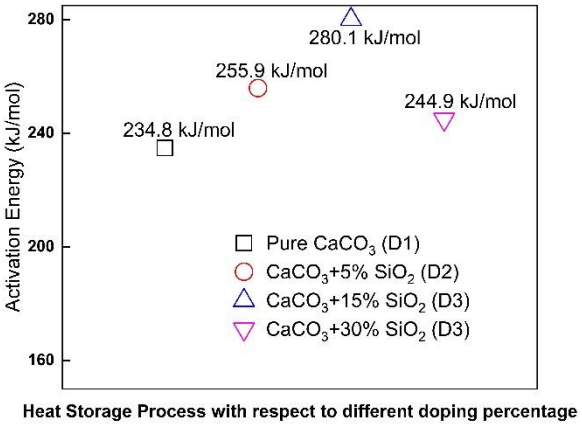

Figure 2. Comparison of activation energy for pure and doped calcium carbonate

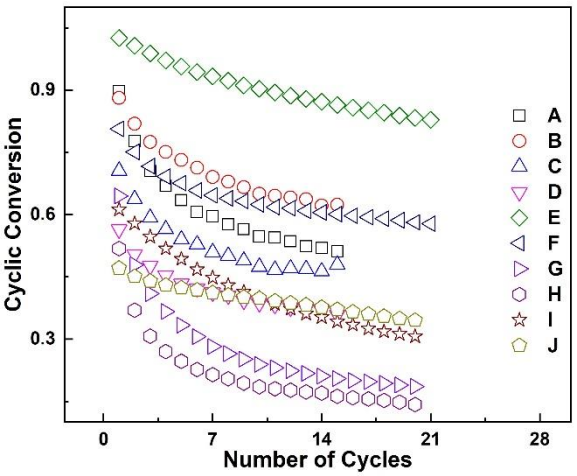

Figure 3. Cyclic conversion of different samples over 15 cycles. A, B, C and D are pure $CaCO_3$, samples doped with 5%, 15% and 30% SiO_2 from current study, respectively. E and F are dolomite and limestone reported by Sarrion [59]. G is for pure $CaCO_3$ and H is for doped with 10% SiO_2 [35]. I and J are for 10% and 30% doped with SiO_2 [60]

4. Conclusion

In this study, SiO_2 is used as a dopant to improve the heat storage efficiency of $CaCO_3$. The kinetics of decarbonation reaction of the pure $CaCO_3$, and 5, 10 and 15% SiO_2-doped thermal composite were studied and all the prepared composite samples were analyzed to determine their volumetric as well as gravimetric thermal energy storage densities. Then, these samples were analyzed using XRD technique to determine their composition and the presence of any new phase for the doped samples. The durability of the samples over 15 cycles was also studied. The conclusions are as follows:

Thermal energy storage density increases when the amount of dopant decreases in the sample, for example gravimetric energy storage densities of 30% and 5% doped samples are 339.85 and 759.24 J/g, respectively. Similarly, volumetric energy storage densities of 30% and 5% doped samples are 155.35 and 54.75 J/mL, respectively. This is because the density of the samples decreases significantly with the increase of the dopant amount.

For the samples with 15% and 30% doping of SiO_2, the CaO produced during decarbonation reaction reacted with SiO_2 and produced Ca_3SiO_5 that introduced a new phase in the calcined material, whereas, no such phase was observed in the samples doped with 5% SiO_2. The new phase (Ca_3SiO_5) was stable, and it did not affect the performance of the material.

The activation energy values were determined as 255.9, 280.1, 244.9 and 234.8 kJ/mol for 5%, 15%, 30% and 0% doped SiO_2 samples, respectively. These values are different because the $CaCO_3$ with different doping of SiO_2 follow different calcination mechanisms. For example, the pure $CaCO_3$ decomposes with D1 model, and 5% doped sample uses D2 model. Similarly, both 15% and 30% doped samples follow the D3 model. Therefore, for the 15% and 30% SiO_2 samples a comparison of activation energies can be performed. The activation energy decreases by 35.2 kJ/mol by increasing loading of dopant from 15 to 30%.

The cyclic stability of the material increases with the increase in dopant amount upto 5%. This happens because dopant controls the particle boundary movement by inducing a Zener pinning force, which leads to low sintering of CaO particles. For higher doping of SiO_2, the cyclic stability reduces. Therefore, it is recommended to use the 5% SiO_2-doped CaCO3 for further exploration for the TCES system.

Acknowledgement

This research work is funded by Jiangsu Excellent Postdoctoral Program (2022ZB638). The authors acknowledge the support and are thankful to the organization. Furthermore, authors are thankful to Prof. C.Y. Zhao from Shanghai Jiao Tong University for his support.

References

[1] UNFCC, Framework Convention on Climate Change.Adoption of the Paris Agreement. Proposal by the President. 2015.

[2] Hinkley, J.T., *et al.*, An analysis of the costs and opportunities for concentrating solar power in Australia, *Renewable Energy*, *57* (2013), pp. 653-661

[3] Siva Reddy, V., *et al.*, State-of-the-art of solar thermal power plants—A review, *Renewable and Sustainable Energy Reviews*, *27* (2013), pp. 258-273

[4] Zhang, H.L., *et al.*, Concentrated solar power plants: Review and design methodology, *Renewable and Sustainable Energy Reviews, 22* (2013), pp. 466-481
[5] Guo, Y., *et al.*, Thermal energy storage using calcium chloride hexahydrate, *Thermal Science, 22* (2018), 6B, pp. 3035-3041
[6] Lokesh, S., *et al.*, Melting/solidification characteristics of paraffin based nanocomposite for thermal energy storage applications, *Thermal Science, 21* (2017), 6A, pp. 2517-2524
[7] Sun, J., *et al.*, Experimental study of a large temperature difference thermal energy storage tank for centralized heating systems, *Thermal Science, 22* (2018), 1B, pp. 613-621
[8] Ledesma, J.T., *et al.*, Numerical simulation of the solar thermal energy storage system for domestic hot water supply located in south spain, *Thermal Science, 17* (2013), pp. 431-442
[9] Shah, N.-u.-H., *et al.*, Thermal analysis of a mini solar pond of small surface area while extracting heat from lower convective layer, *Thermal Science, 23* (2019), 2A, pp. 763-776
[10] John, M.R.W., *et al.*, Waste heat recovery from diesel engine using custom designed heat exchanger and thermal storage system with nanoenhanced phase change material, *Thermal Science, 21* (2017), 1B, pp. 715-727
[11] Bauer, T., *et al.*, Overview of molten salt storage systems and material development for solar thermal power plants, *Proceedings*, SOLAR 2012, Denver, 2012
[12] Parrado, C., *et al.*, 2050 LCOE improvement using new molten salts for thermal energy storage in CSP plants, *Renewable and Sustainable Energy Reviews, 57* (2016), pp. 505-514
[13] Liu, M., *et al.*, Review on concentrating solar power plants and new developments in high temperature thermal energy storage technologies, *Renewable and Sustainable Energy Reviews, 53* (2016), pp. 1411-1432
[14] Pfleger, N., *et al.*, Thermal energy storage–overview and specific insight into nitrate salts for sensible and latent heat storage, *Beilstein journal of nanotechnology, 6* (2015), 1, p. 1487-1497
[15] Janz, G.J., *et al.*, Physical properties data compilations relevant to energy storage. II. Molten salts: data on single and multi-component salt systems, *National Standard Reference Data System*, (1979)
[16] Mehmood, T., *et al.*, Simplified mathematical model and experimental analysis of latent thermal energy storage for concentrated solar power plants, *Journal of Energy Storage, 41* (2021)
[17] Steinmann, W.-D. and C. Prieto, 24-Thermal storage for concentrating solar power plants, in: *Advances in Thermal Energy Storage Systems (Second Edition)* (Ed. L.F. Cabeza), Woodhead Publishing, 2021, pp. 673-697
[18] Xu, B., P. Li, and C. Chan, Application of phase change materials for thermal energy storage in concentrated solar thermal power plants: A review to recent developments, *Applied Energy, 160* (2015), pp. 286-307
[19] Elmozughi, A.F., *et al.*, Encapsulated phase change material for high temperature thermal energy storage – Heat transfer analysis, *International Journal of Heat and Mass Transfer, 78* (2014), pp. 1135-1144
[20] Asgharian, H. and E. Baniasadi, A review on modeling and simulation of solar energy storage systems based on phase change materials, *Journal of Energy Storage, 21* (2019), pp. 186-201
[21] Tao, Y.B. and Y.-L. He, A review of phase change material and performance enhancement method for latent heat storage system, *Renewable and Sustainable Energy Reviews, 93* (2018), pp. 245-259
[22] Gil, A., *et al.*, State of the art on high temperature thermal energy storage for power generation. Part 1—Concepts, materials and modellization, *Renewable and Sustainable Energy Reviews, 14* (2010), 1, pp. 31-55
[23] Paksoy, H.Ö., Thermal energy storage for sustainable energy consumption: fundamentals, case studies and design, *Proceedings*, Springer Science & Business Media, 2007, Vol. 234
[24] Mahlia, T., *et al.*, A review of available methods and development on energy storage; technology update, *Renewable and Sustainable Energy Reviews, 33* (2014), pp. 532-545
[25] Pardo, P., *et al.*, A review on high temperature thermochemical heat energy storage, *Renewable and Sustainable Energy Reviews, 32* (2014), pp. 591-610
[26] Wentworth, W. and E. Chen, Simple thermal decomposition reactions for storage of solar thermal energy, *Solar Energy, 18* (1976), 3, pp. 205-214

[27] Sakellariou, K.G., *et al.*, Calcium oxide based materials for thermochemical heat storage in concentrated solar power plants, *Solar Energy, 122* (2015), pp. 215-230
[28] Ervin, G., Solar heat storage using chemical reactions, *Journal of solid state chemistry, 22* (1977), 1, pp. 51-61
[29] Perejón, A., *et al.*, On the relevant role of solids residence time on their CO_2 capture performance in the Calcium Looping technology, *Energy, 113* (2016), pp. 160-171
[30] N'Tsoukpoe, K.E., *et al.*, The size of sorbents in low pressure sorption or thermochemical energy storage processes, *Energy, 77* (2014), pp. 983-998
[31] Lee, M.g., *et al.*, Mineral carbonation of flue gas desulfurization gypsum for CO_2 sequestration, *Energy, 47* (2012), 1, pp. 370-377
[32] Duelli, G., *et al.*, Investigations at a 10kWth calcium looping dual fluidized bed facility: Limestone calcination and CO_2 capture under high CO_2 and water vapor atmosphere, *International Journal of Greenhouse Gas Control, 33* (2015), pp. 103-112
[33] Shui, M., *et al.*, The decomposition kinetics of the SiO_2 coated nano-scale calcium carbonate. *Thermochimica Acta, 386* (2002), 1, pp. 43-49
[34] Kumar, D., *et al.*, Decomposition kinetics of $CaCO_3$ dry coated with nano-silica, *Thermochimica Acta, 624* (2016), pp. 35-46
[35] Chen, X., *et al.*, Experimental investigation on the $CaO/CaCO_3$ thermochemical energy storage with SiO_2 doping, *Energy, 155* (2018), pp. 128-138
[36] Valverde, J.M., *et al.*, Effect of Thermal Pretreatment and Nanosilica Addition on Limestone Performance at Calcium-Looping Conditions for Thermochemical Energy Storage of Concentrated Solar Power, *Energy & Fuels, 31* (2017), 4, pp. 4226-4236
[37] Yanase, I., *et al.*, The effect of addition of a large amount of CeO_2 on the CO_2 adsorption properties of CaO powder, *Chemical Engineering Journal, 327* (2017), pp. 548-554
[38] Jin, D., *et al.*, Decomposition kinetics study of AlOOH coated calcium carbonate, *Materials Chemistry and Physics, 115* (2009), 1, pp. 418-422
[39] Barker, R., The reversibility of the reaction $CaCO_3 \rightleftarrows CaO + CO_2$, *Journal of Applied Chemistry and Biotechnology, 23* (1973), 10, pp. 733-742
[40] Erans, M., *et al.*, Calcium looping sorbents for CO_2 capture, *Applied Energy, 180* (2016), pp. 722-742
[41] Lu, S. and S. Wu, Calcination–carbonation durability of nano $CaCO_3$ doped with Li_2SO_4, *Chemical Engineering Journal, 294* (2016), pp. 22-29
[42] Jing, J.-y., *et al.*, Enhanced CO_2 sorption performance of $CaO/Ca_3Al_2O_6$ sorbents and its sintering-resistance mechanism, *Applied Energy, 199* (2017), pp. 225-233
[43] Wang, Y., *et al.*, A new nano CaO-based CO_2 adsorbent prepared using an adsorption phase technique, *Chemical Engineering Journal, 218* (2013), pp. 39-45
[44] Benitez-Guerrero, M., *et al.*, Large-scale high-temperature solar energy storage using natural minerals, *Solar Energy Materials and Solar Cells, 168* (2017), pp. 14-21
[45] Chen, H., *et al.*, Reactivity enhancement of calcium based sorbents by doped with metal oxides through the sol–gel process, *Applied Energy, 162* (2016), pp. 390-400
[46] Wikipedia, Lithium sulfate, https://en.wikipedia.org/wiki/Lithium_sulfate
[47] Application of magnesium compounds to insulating heat-conductive fillers, https://web.archive.org/web/20131230233440/http://www.konoshima.co.jp/en/resdev/004.html
[48] Haynes, W.M., *CRC handbook of chemistry and physics*, CRC press, 92nd ed., 2011
[49] Wikipedia, Manganese dioxide, https://en.wikipedia.org/wiki/Manganese_dioxide
[50] Xie, H., *et al.*, MgO nanofluids: higher thermal conductivity and lower viscosity among ethylene glycol-based nanofluids containing oxide nanoparticles, *Journal of Experimental Nanoscience, 5* (2010), 5, pp. 463-472
[51] Valverde, J., *et al.*, Enhancement of fast CO_2 capture by a nano-SiO_2/CaO composite at Ca-looping conditions, *Environmental Science & Technology, 46* (2012), 11, pp. 6401-6408
[52] Wang, M., *et al.*, Absorption of CO_2 on $CaSiO_3$, *Proceedings*, The 2008 Annual Meeting, 2008
[53] Khosa, A.A. and C.Y. Zhao, Heat storage and release performance analysis of $CaCO_3$/CaO thermal energy storage system after doping nano silica, *Solar Energy, 188* (2019), pp. 619-630
[54] Wang, M. and C.-G. Lee, Absorption of CO_2 on $CaSiO_3$ at high temperatures, *Energy Conversion and Management, 50* (2009), 3, pp. 636-638

[55] Khosa, A.A., *et al.*, Investigating the effects of ZnO dopant on the thermodynamic and kinetic properties of $CaCO_3$/CaO TCES system, *Energy, 215* (2021)
[56] Vyazovkin, S., *et al.*, ICTAC Kinetics Committee recommendations for performing kinetic computations on thermal analysis data, *Thermochimica acta, 520* (2011), 1-2, pp. 1-19
[57] Coats, A.W. and J. Redfern, Kinetic parameters from thermogravimetric data. *Nature, 201* (1964), 4914
[58] Achar, B.N., *et al.*, Kinetics and mechanism of dehydroxylation processes: III. Applications and limitations of dynamic methods, *Proceeding*, Int. Clay Conf. Jerusalem. 1966
[59] Sarrion, B., *et al.*, On the multicycle activity of natural limestone/dolomite for thermochemical energy storage of concentrated solar power, *Energy Technology, 4* (2016), 8, pp. 1013-1019
[60] Benitez-Guerrero, M., *et al.*, Low-cost Ca-based composites synthesized by biotemplate method for thermochemical energy storage of concentrated solar power, *Applied Energy, 210* (2018), pp. 108-116

Submitted: 22.04.2023.
Revised: 19.06.2023.
Accepted: 23.06.2023.